Published in final edited form as:
Chem Commun (Camb). 2010 September 28; 46(36): 6684–6686. doi:10.1039/c0cc01041c.

HSA coated MnO nanoparticles with prominent MRI contrast for tumor imaging†

Jing Huang[a,b,‡], **Jin Xie**[a,c,‡], **Kai Chen**[a], **Lihong Bu**[a,d], **Seulki Lee**[a,c], **Zhen Cheng**[a], **Xingguo Li**[b], and **Xiaoyuan Chen**[a,c]

Xingguo Li: xgli@pku.edu.cn; Xiaoyuan Chen: shawn.chen@nih.gov

[a]Department of Radiology and Bio-X Program, Stanford University, 1201 Welch Road P087, Stanford, CA 94305, USA

[b]Beijing National Laboratory for Molecular Sciences (BNLMS), College of Chemistry and Molecular Engineering, Peking University, Beijing 100871, P.R. China

[c]Laboratory of Molecular Imaging and Nanomedicine (LOMIN), National Institute of Biomedical Imaging and Bioengineering (NIBIB), National Institutes of Health (NIH), Bethesda, MD 20892, USA

[d]Department of Radiology, The Fourth Hospital of Harbin Medical University, Heilongjiang, 150001, P.R. China

Abstract

We report in this Communication a facile, two-step surface modification strategy to achieve manganese oxide nanoparticles with prominent MRI T1 contrast. In a U87MG glioblastoma xenograft model, we confirmed that the particles can accumulate efficiently in tumor area to induce effective T1 signal alteration.

Inorganic magnetic nanoparticles have emerged as an important class of biomaterials. Iron oxide nanoparticles, for instance, have been intensively studied as MRI contrast agents to improve T_2 image quality,[1–5] and several formulas have advanced into clinical trial or passed FDA approval.[6–9] Compared with the rapid pace of T_2 probe development, research progress in developing magnetic nanoparticle based T_1 probes has been rather slow.[10] In clinical practice, T_1 contrast agents are mostly metal-chelator complexes, such as Gd-DTPA (Magnevist). Magnetic nanoparticles, each constructed with thousands of metal atoms, are potentially advantageous for longer circulation half-life and better contrast; however, their translation into practice has been hampered, in large part due to the lack of a reliable surface coating technique that can render particles with sufficient stability, without compromising the contrast effect. Previously, the Hyeon group reported the use of MnO nanoparticles (MONPs) as T_1 contrast agents for brain imaging.[11] In that study, the MONPs, originally synthesized by pyrolysis with a thick hydrocarbon layer, were rendered water soluble by adding one layer of phospholipid. However, such paramagnetic T_1 relaxation enhancement is a spin–lattice effect, which requires direct contact between surface Mn and water. The dilayer structure, with a thick hydrophobic hydrocarbon inner coating, is potentially inhibitive of water penetration, which may explain the relatively low r_1 relaxivity of the phospholipid-coated MONPs (0.21 s^{-1} mM^{-1} for particles with 20 nm core.[12])

†Electronic supplementary information (ESI) available: Details of nanoparticle preparation and *in vivo* studies. See DOI: 10.1039/c0cc01041c

Correspondence to: Xingguo Li, xgli@pku.edu.cn; Xiaoyuan Chen, shawn.chen@nih.gov.

‡These authors contributed equally to this work.

Here we report a facile, two-step surface modification strategy to make water-soluble MONPs with much improved T1 contrast; we also confirm that the particles can accumulate in the tumor area of a U87MG glioblastoma xenograft model and induce an effective T_1 signal. We have previously reported a similar surface modification strategy to modify iron oxide nanoparticles.[13,14] In the current instance, we first synthesized MONPs, which were coated with oleic acid, using a pyrolysis method.[11,15,16] These water-insoluble particles were then dispersed in a 1 : 1 $CHCl_3$/DMSO mixture solution, incubated and surface-exchanged with dopamine.[13,17] The DMSO solution of dopamine coated MONPs was added dropwise to a human serum albumin (HSA) aqueous solution. Owing to the superior ligand binding capacity of HSA,[18,19] as well as the post-modification amine-rich particle surface,[14] the HSA was efficiently adsorbed onto the particle surface, where it conferred extra stability to the particles (Fig. 1). Protein assay and ICP analysis revealed that there were about 10 HSA molecules on each MONP, similar to the previous observation with HSA coated Fe_3O_4 NPs.[13]

Fig. 2a is a representative TEM image of the as-synthesized MONPs in hexane. It shows that the MONPs have a core size of about 20 nm, similar to what was previously reported.[11,12] The TEM image shown in Fig. 2b was taken after the MONPs received surface modification and were added to water. No agglomeration of particles was found in the examined area, suggesting good dispersibility of the particles. Meanwhile, no morphological changes were found between Fig. 2a and b, indicating minimal damage caused by the surface modification. The overall size of the MONPs increased from 25.2 ± 1.9 to 39.2 ± 3.6 nm (Fig. 2c), as characterized by dynamic light scattering (DLS), which we attributed to the addition of the HSA coating. Similar to the case of HSA coated Fe_3O_4 nanoparticles, long-term stability of HSA-MONPs in aqueous solution was observed, as no obvious size change was found during a 48 h incubation period (in PBS, 37 °C) (Fig. 2d).

To evaluate the T_1 contrast effect, the following were compared in an MRI phantom study: (1) HSA-MONPs, (2) phospholipid (1,2-distearoyl-sn-glycero-3-phosphoethanolamine- N-[methoxy(polyethylene glycol)-2000]) coated MONPs (DSPE-MONPs).[11] The samples were prepared by dispersing particles at pre-determined Mn concentrations in 1% agarose gel. As shown in Fig. 3, the HSA-MONPs induced stronger signal increases at all Mn concentrations than DSPE-MONPs. Based on the imaging results, the r_1 relaxivity of DSPE-MONPs was found to be 0.37 mM^{-1} s^{-1}, similar to the previous reported value.[12] On the other hand, r_1 of HSA-MONPs was evaluated to be 1.97 mM^{-1} s^{-1}, which was five times higher than that of DSPE-MONPs. Since the starting materials were the same, this increase was attributed to the unique dopamine-HSA coating. Indeed, compared with the phospholipid coating, where MONPs were surrounded by a hydrophobic inner layer that may isolate the cores from their surroundings, the dopamine coating, being more hydrophilic and compact, may allow more efficient water exchange.

The physiology stability and superior contrast make such particles useful as T_1 contrast agents. Previously, we have demonstrated that HSA coated Fe_3O_4 nanoparticles can accumulate at tumor areas through an enhanced permeability and retention (EPR) effect.[13] We expect that the HSA-MONPs, with the same coating strategy and similar hydrodynamic size, may possess similar pharmacokinetics. To understand the particle distribution better, we labeled the HSA-MONPs with ^{64}Cu-DOTA chelator, and used PET/MRI dual modality imaging to study their *in vivo* particle distribution. The details of DOTA coupling and ^{64}Cu labeling can be found in the Supporting Information, as well as in our previous publications.[13,20] The imaging studies were performed in a U87MG xenograft model. It was prepared by subcutaneously inoculating 5×10^6 U87MG cells in 100 μl PBS into the front flank of each mouse, and the imaging was performed about 3 weeks later when the tumor reached a size of 100 mm^3. All animal work was conducted following a protocol approved

by the Stanford University Administrative Panel on Laboratory Animal Care (APLAC). For imaging, ^{64}Cu labeled HSA-MONPs in PBS, at a dose of 10 mg Mn/kg, were administrated intravenously (i.v.), and PET and T_1-weighted MRI images were acquired at 1, 4, and 24 h post injection (p.i.) (ESI†). The lower panel of Fig. 4 gives the PET results. The activities in tumor started to be visualized at the 1 h time point, at an uptake of 3.3 ± 0.4%ID/g (n = 3). Such tumor accumulation peaked at 4 h p.i. (4.7 ± 0.4%ID/g), and slightly decreased to 4.3 ± 0.2%ID/g at 24 h. This profile correlated well with the T_1-weighted MRI observation. Compared to those before MONP injection, the MRI signals in tumor increased by 5.3 ± 0.6%, 13.8 ± 2.0% and 9.7 ± 2.1% at 1, 4, 24 h p.i. (n = 3, the upper panel of Fig. 4), respectively. These correlated imaging profiles from both modalities validated the accumulation of MONPs in the tumor area. The signal drops at late time points, observed in both PET and MRI results, were likely caused by the slow washout of the tracers, which is common in EPR mediated tumor targeting. These observations suggested a reasonably long circulation half life of the HSA-MONPs, with an optimal observation window at around 4 h.

Immediately after imaging at the 24 h time point, the mice were sacrificed, and the tumor and major organs were collected and subjected to an *ex vivo* PET scan (Fig. 5a). In accord with the *in vivo* observations, strong activities were found in the tumor. Meanwhile, high tracer accumulation was also found in the liver, which is not surprising considering the overall size of the HSA-MONPs.[6,13]

To further confirm that the particles indeed accumulated in the tumor and liver, we used TEM to examine the tissue samples taken from animal models after imaging at the 4 h time point. As displayed in Fig. 5b–d, many MONPs (black dots in white circles) were found across the liver and tumor samples. Notably, the particles in the liver were mostly found within cells, likely due to engulfment by Kupffer cells, and were distributed in the tissue in a relatively homogeneous fashion. On the other hand, the MONPs in the tumor were found both inside and outside of cells. Such a distribution pattern was reminiscent of our previous observation with HSA coated Fe_3O_4 nanoparticles, where some particles were found trapped at the interstitial space in the tumor after extravasation.[13]

In summary, we have developed a novel method to modify pyrolysis-yielded MONPs. Such a strategy, with a compact and hydrophilic coating, allows more efficient water-surface interaction and, therefore, leads to more prominent T_1 contrast. As a proof-of-concept study, we coupled such nanoparticles with ^{64}Cu radioisotope and performed PET/MRI dual imaging in a U87MG xenograft model. Good tumor accumulation was observed by both imaging modalities and was confirmed by *ex vivo* PET and TEM assessment. The current formulation shows an r_1 of 1.97 mM^{-1} s^{-1}, which is close but inferior to Magnevist (about 5 mM^{-1} s^{-1}). However, the good tumor targeting and the excellent ligand binding capacity by the HSA coating yet make them a promising imaging or theranostic platform. In addition, we anticipate even better T_1 contrast effect in the future using smaller, hollow-structured MONPs as the core. The related research is underway.

Supplementary Material

Refer to Web version on PubMed Central for supplementary material.

Acknowledgments

This research was supported by Intramural Research Programs of the National Institute of Biomedical Imaging and Bioengineering (NIBIB) and MOST of China (No. 2009CB939902 and 2010CB631301).

Notes and references

1. Lee HY, Li Z, Chen K, Hsu AR, Xu C, Xie J, Sun S, Chen X. J Nucl Med. 2008; 49:1371–1379. [PubMed: 18632815]
2. Xie J, Chen K, Lee HY, Xu C, Hsu AR, Peng S, Chen X, Sun S. J Am Chem Soc. 2008; 130:7542–7543. [PubMed: 18500805]
3. Chen K, Xie J, Xu H, Behera D, Michalski MH, Biswal S, Wang A, Chen X. Biomaterials. 2009; 30:6912–6919. [PubMed: 19773081]
4. Jun YW, Huh YM, Choi JS, Lee JH, Song HT, Kim S, Yoon S, Kim KS, Shin JS, Suh JS, Cheon J. J Am Chem Soc. 2005; 127:5732–5733. [PubMed: 15839639]
5. Lee JH, Huh YM, Jun Y, Seo J, Jang J, Song HT, Kim S, Cho EJ, Yoon HG, Suh JS, Cheon J. Nat Med. 2007; 13:95–99. [PubMed: 17187073]
6. Xie J, Huang J, Li X, Sun S, Chen X. Curr Med Chem. 2009; 16:1278–1294. [PubMed: 19355885]
7. Ito A, Shinkai M, Honda H, Kobayashi T. J Biosci Bioeng. 2005; 100:1–11. [PubMed: 16233845]
8. Jun YW, Seo JW, Cheon A. Acc Chem Res. 2008; 41:179–189. [PubMed: 18281944]
9. Harisinghani MG, Barentsz J, Hahn PF, Deserno WM, Tabatabaei S, van de Kaa CH, de la Rosette J, Weissleder R. N Engl J Med. 2003; 348:2491–2499. [PubMed: 12815134]
10. Guo K, Berezin MY, Zheng J, Akers W, Lin F, Teng B, Vasalatiy O, Gandjbakhche A, Griffiths GL, Achilefu S. Chem Commun. 2010; 46:3705–3707.
11. Na HB, Lee JH, An K, Park YI, Park M, Lee IS, Nam DH, Kim ST, Kim SH, Kim SW, Lim KH, Kim KS, Kim SO, Hyeon T. Angew Chem, Int Ed. 2007; 46:5397–5401.
12. Shin J, Anisur RM, Ko MK, Im GH, Lee JH, Lee IS. Angew Chem, Int Ed. 2009; 48:321–324.
13. Xie J, Chen K, Huang J, Lee S, Wang J, Gao J, Li X, Chen X. Biomaterials. 2010; 31:3016–3022. [PubMed: 20092887]
14. Xie J, Wang J, Niu G, Huang J, Chen K, Li X, Chen X. Chem Commun. 2010; 46:433–435.
15. Na HB, Lee JH, An KJ, Park YI, Park M, Lee IS, Nam DH, Kim ST, Kim SH, Kim SW, Lim KH, Kim KS, Kim SO, Hyeon T. Angew Chem, Int Ed. 2007; 46:5397–5401.
16. Park J, An KJ, Hwang YS, Park JG, Noh HJ, Kim JY, Park JH, Hwang NM, Hyeon T. Nat Mater. 2004; 3:891–895. [PubMed: 15568032]
17. Xie J, Xu C, Kohler N, Hou Y, Sun S. Adv Mater. 2007; 19:3648–3652.
18. Gradishar WJ. Expert Opin Pharmacother. 2006; 7:1041–1053. [PubMed: 16722814]
19. Kratz F. J Controlled Release. 2008; 132:171–183.
20. Li ZB, Cai W, Cao Q, Chen K, Wu Z, He L, Chen X. J Nucl Med. 2007; 48:1162–1171. [PubMed: 17574975]

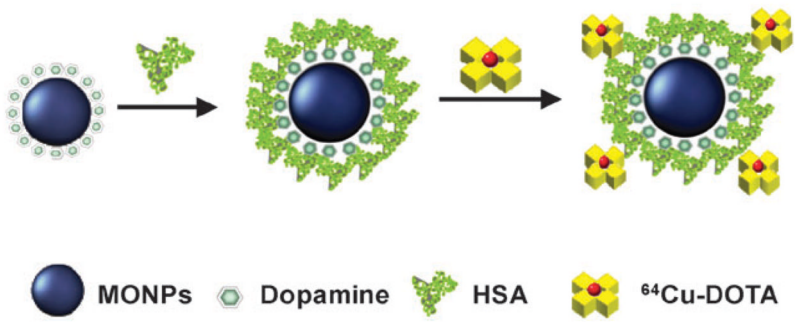

Fig. 1.
Schematic illustration of the formation of HSA-MONPs.

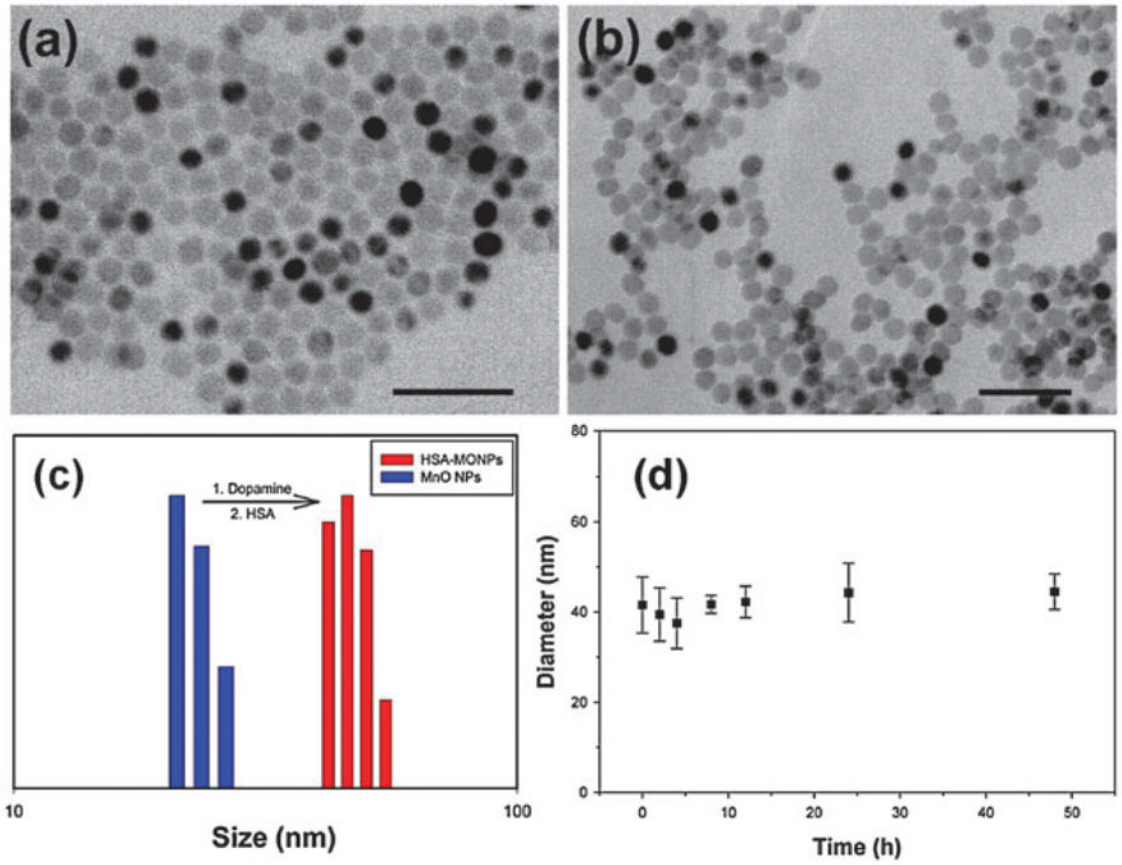

Fig. 2.

TEM images of (a) as-synthesized MONPs dispersed in hexane and (b) HSA-MONPs in water. Scale bars are 100 nm. (c) Hydrodynamic size of MONPs before and after modification. (d) Size change of HSA-MONPs when incubated in PBS at 37 °C for 48 h, monitored by DLS.

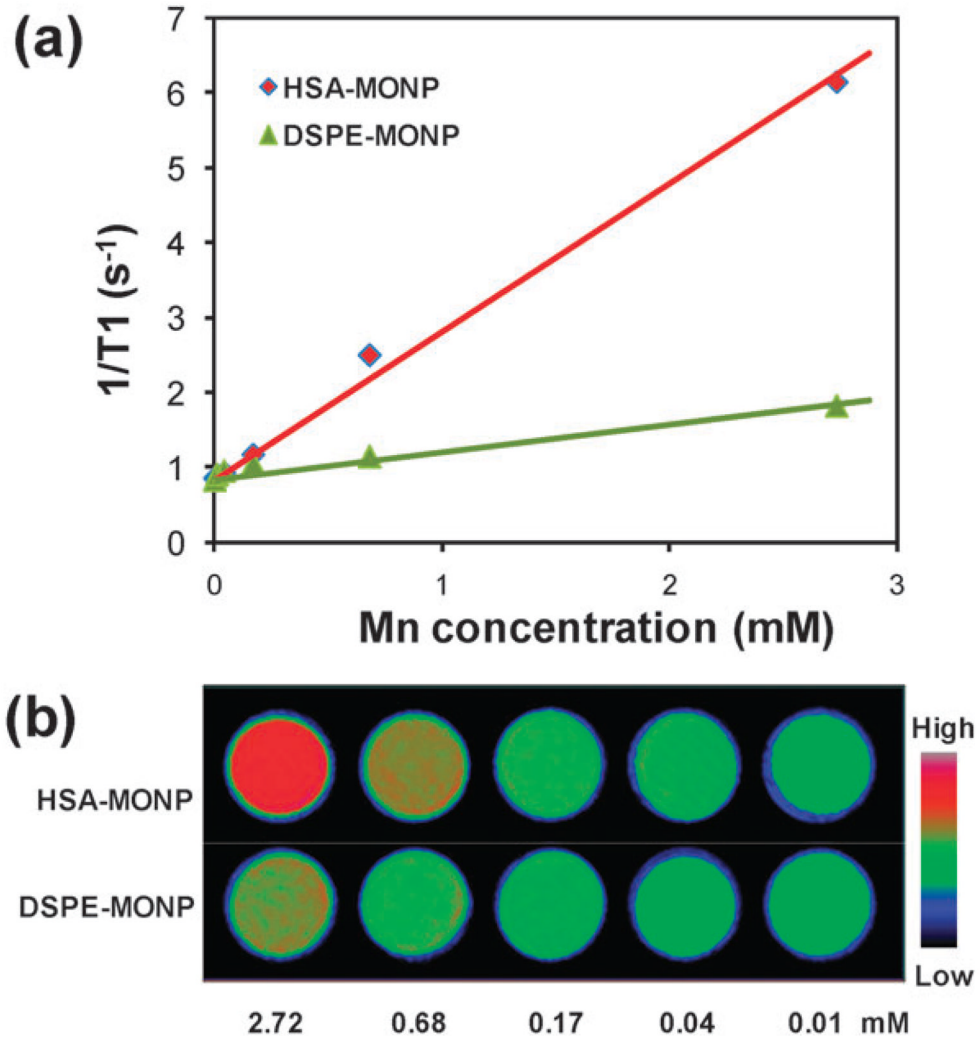

Fig. 3.

(a) $1/T_1$ *vs.* Mn concentration curves of HSA- and DSPE-MONPs. The slopes, *i.e.* the r_1 values, were evaluated to be 1.97 and 0.37 mM^{-1} s^{-1}, respectively. (b) T_1-weighted MR images of MONPs in aqueous solution with various concentrations.

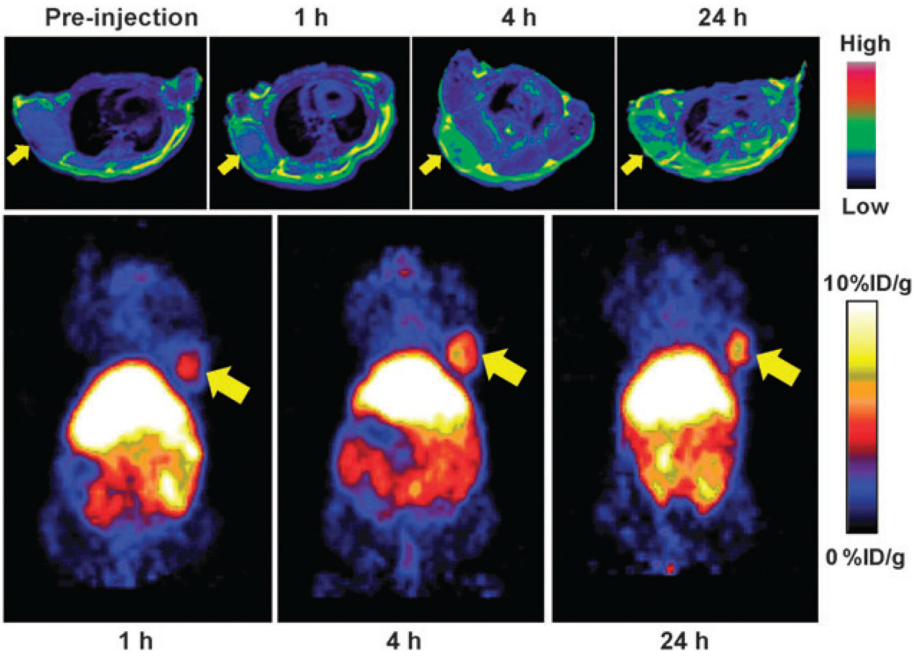

Fig. 4.

Upper panel: MR images on U87MG xenograft animal model acquired at 0, 1, 4 and 24 h after ^{64}Cu-HSA-MONPs injection. Lower panel: PET images taken at 1, 4 and 24 h after ^{64}Cu-HSA-MONP injection.

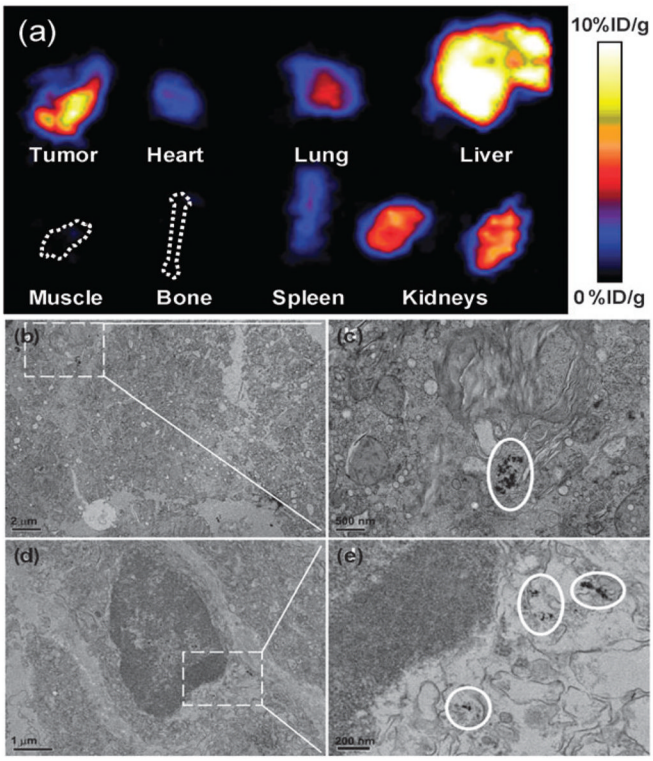

Fig. 5.

(a) *Ex vivo* PET imaging on tumor and major organs after 24 h imaging. (b–e), TEM images taken on liver and tumor samples from animal models after 4 h imaging. (b) and (c), TEM images of the liver tissue samples. (d) and (e) TEM images of the tumor tissue samples.